

# Multivariable controller design for an industrial distillation column

F. Allgöwer                      J. Raisch

## Abstract

In this paper, we report our experience with the design of linear multivariable controllers for a staged binary distillation column with 40 trays. Controller design methods include  $H_\infty$ -minimization, DNA-design, CL-design and  $H_2$ -minimization. Results obtained at the real plant are shown.

## 1 Introduction

Distillation is one of the most important processes in the chemical industries. In distillation columns, a mixture of chemical substances is separated into products that are more valuable. Control of distillation columns is essential to meet product specifications, to reduce investment and energy costs and to limit environmental impact. These goals can be achieved by maintaining product purities within given bounds.

The column considered in this paper is a staged binary column with 40 trays, which satisfies industrial standards.

In the sequel, a number of linear multivariable controllers and a conventional proportional-integral controller are designed for this column. For multivariable design, we use  $H_\infty$ - and  $H_2$ -minimization method [2] [3] [11], the Characteristic Locus method [4] and the Direct Nyquist Array method [9]. We are especially interested in assessing the effort needed to get a 'good' controller: That is, of course, closely related to the question of how easily engineering specifications can be included in the design process.

This paper is restricted to binary separation. The same methods, however, can be used to control multi-component distillation columns.

## 2 The plant

### 2.1 The distillation column

The high-purity distillation plant to be controlled is a staged column for the separation of a binary mixture. It operates continuously and consists of 40 trays, a condenser and a reboiler. The column is in pilot plant scale and satisfies industrial standards (Table 2.1.1).

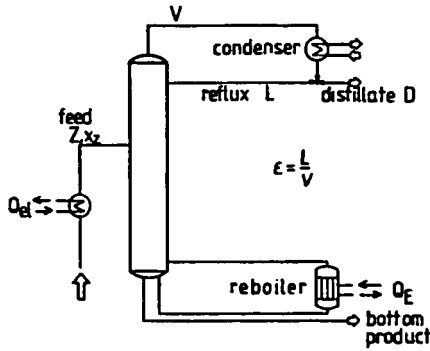


Figure 2.1.1. Schematic representation of the distillation column

The column exhibits most of the problems that appear in industrial binary distillation and is therefore well suited to test controllers under realistic conditions.

As an example, we consider a mixture of two alcohols, methanol and propanol, that is to be separated. Propanol is the high-boiling residue and therefore removed at the base, methanol is the light-boiling distillate and is withdrawn at the column head.

material	glass
trays	40 tubble cap trays, 10cm diameter
height	10cm
reboiler	electrically heated 0 to 12KW, level controlled
condenser	water cooled, level controlled
pressure	atmospheric
feed	on tray 12 (numbered from the top), electrically preheated
preheater	with temperature control
heatjacket	12 sectors independently controlled

Table 2.1.1: Technical data of the plant

The fractioning tower is heated from below with the energy flow  $Q_E$ , which is used as one manipulated variable. The second manipulated variable is the reflux-ratio  $\epsilon$ , the ratio between reflux flow  $L$  and vapor flow  $V$  (Figure 2.1.1). There are temperature sensors on each tray and a process-chromatograph at the head to measure the concentration of one component there.

The column is divided into two parts, namely the stripping section at the base and the enrichment section above it. The mixture to be seperated is fed into the fractioning tower as a continuous stream, the feed  $Z$ , between stripping and enrichment section. Before entering the column, the feed is electrically preheated to a constant temperature (Figure 2.1.1).

The most important disturbances that occur in practice are changes in flow  $Z$  and feed composition  $x_z$ . These two disturbances are considered in this paper.

## 2.2 The nonlinear model

The dynamic behaviour of the distillation column can be described fairly accurately by a mixed set of differential and algebraic equations.

The nonlinear model is based on the following assumptions:

- neglected hold-up of the vapor phase
- ideal stages, i.e., the mixture is at equilibrium temperature on each tray (Murphree efficiency is introduced to correct errors resulting from this assumption)
- hydrodynamical effects are neglected
- the volume of the liquid on each stage is considered to be a constant

Material balances, energy balances and thermodynamical correlations for each stage then yield a set of 320 nonlinear differential and algebraic equations.

To give a flavour of the severe nonlinearities, the calculation of the boiling-point equilibrium is shown as an example:

$$y_{ik} = y_{i, k+1} + E(y_{ik}^* - y_{i, k+1}) \quad (2.2.1)$$

where

$$y_i^* = \frac{p_{is}(T)}{p} \gamma_i x_i, \quad i = 1, 2 \quad (2.2.2)$$

$$\sum_{i=1}^2 y_i^* = 1 \quad (2.2.3)$$

The activity coefficients  $\gamma_i$  are due to Wilson

$$\ln \gamma_i = -\ln \sum_{j=1}^2 x_j \Gamma_{ij} + 1 - \sum_{j=1}^2 \frac{x_j \Gamma_{ji}}{\sum_{l=1}^2 x_l \Gamma_{jl}}, \quad i = 1, 2 \quad (2.2.4)$$

and the saturation vapor pressure  $p_{is}(T)$  is due to Antoine

$$p_{is}(T) = e^{A_i - \frac{B_i}{T+C_i}}, \quad i = 1, 2. \quad (2.2.5)$$

where:

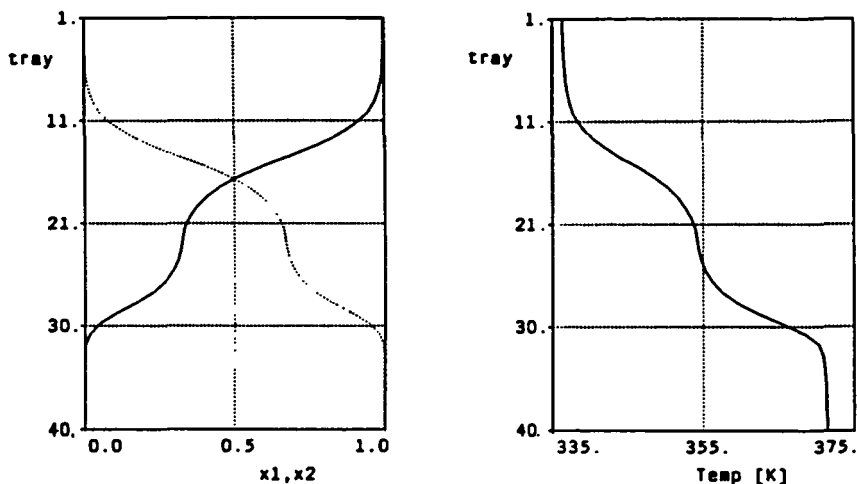


Figure 2.3.1. Concentration and temperature profiles of the stationary column

$y_i$	...	vapor concentration of the $i^{\text{th}}$ component
$y_i^*$	...	vapor concentration of the $i^{\text{th}}$ component at equilibrium
$p$	...	total pressure
$x_i$	...	liquid concentration of the $i^{\text{th}}$ component
$T$	...	temperature in Kelvin
$\Gamma_{nm}$	...	Wilson-parameter
$A_i$	}	...
$B_i$		
$C_i$		

Models of the reboiler and the condenser consist of another 7, respectively 5, nonlinear equations. Thus a set of 332 nonlinear algebraic-differential equations describes the dynamic behaviour.

## 2.3 Nonlinear simulation

Based on the nonlinear dynamic equations referred to in Chapter 2.2, a rather accurate nonlinear simulation of the column is possible. The software package DIVA (Dynamicische SIMulation Verfahrenstechnischer Anlagen [5]) was used for simulation.

Dynamic behaviour of the uncontrolled plant can be understood best from concentration- and temperature-profiles along the vertical axis of the column. Figure 2.3.1 shows the profiles of the stationary column.

In binary separation, the temperature on each stage is 1-to-1 to the concentration on that stage. Therefore, considering only temperature profiles and responses is

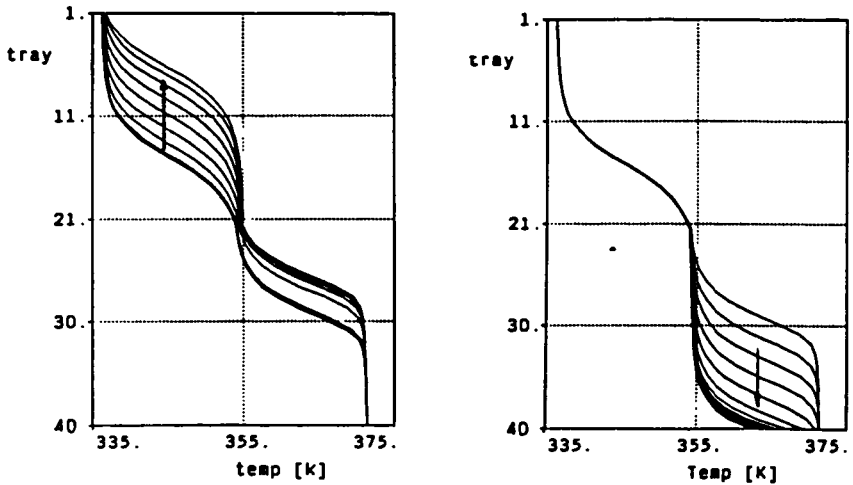


Figure 2.3.2. Responses to step changes of the reflux-ratio by -1% and of the feed flow by +20% (temperature-profiles)

sufficient. Qualitative behaviour of the column due to changes in the manipulated variable ( $Q_E, \epsilon$ ) and changes in the disturbances (feed flow and feed composition) can be described by a movement of the entire profile either towards the head or towards the bottom of the column (plus slight changes in the shape of the profile) [8].

As an example, the effects of a -1% step change of the reflux-ratio and a +20% step change of the feed flow are shown in Figure 2.3.2. A good controller should keep the profile nearly stationary in the presence of disturbances. It is obvious that the product specifications, namely high purity at the top and bottom of the column, are met this way.

If the profile is nearly stationary, we observe largest temperature variations on the 14th and 28th stage. Therefore, temperatures on these stages, which are approximately located at the points of inflection of the profile, are taken as measurements ( $T_{14}, T_{28}$ ). Figure 2.3.3 shows temperature time responses on these stages corresponding to Figure 2.3.2. (Throughout the paper, temperature is measured in Kelvin K, energy flow  $Q_E$  in Kilowatt [KW]).

Additional temperature measurements on other stages improve information about process dynamics only slightly. This is especially true for temperature sensors at the top and bottom stages, which would give direct knowledge of distillate and bottom concentration theoretically. [6]

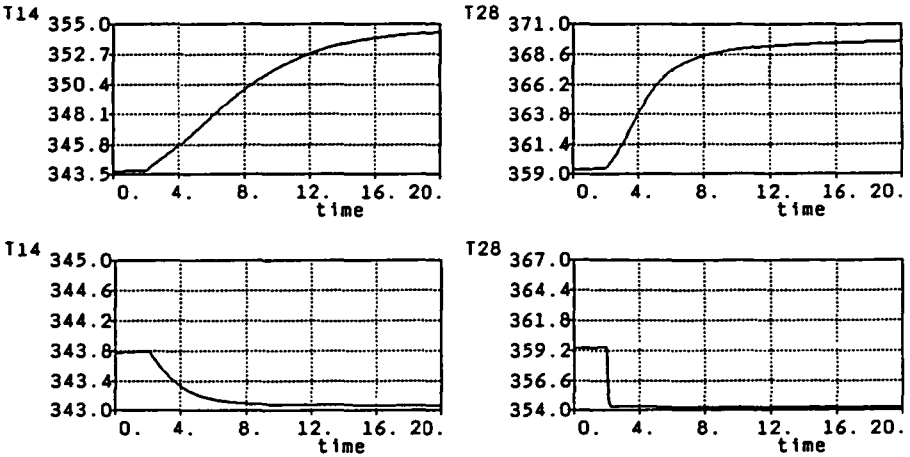


Figure 2.3.3. Temperature time responses on the 14th and 28th tray to a -1% step change of the reflux-ratio and a +20% step change of the feed flow

## 2.4 Plant specifications

By inspection of nonlinear simulation results, sufficient purity of bottom product and distillate is guaranteed, if temperature variations from the set points  $T_{14}^{stat} = 343.8K$  and  $T_{28}^{stat} = 359.4K$  are restricted to certain bounds  $T_{14}^{min}$ ,  $T_{14}^{max}$  and  $T_{28}^{min}$ ,  $T_{28}^{max}$ . Set point changes are not of practical importance and therefore not considered here.

In simulation, the appropriate steady-state value of the energy flow  $Q_E$  is 2.48KW. Maximal and minimal admissible values are  $Q_E^{max} = 12KW$  and  $Q_E^{min} = 2KW$ . Additionally, changes in  $Q_E$  should not be too sudden, because the energy flow can be affected only indirectly (lag-element with a time constant of about 3 minutes).

Due to actuator saturation only reflux-ratios between  $\epsilon^{min} = 0.16$  and  $\epsilon^{max} = 0.65$  are acceptable. In simulation, the steady-state reflux-ratio is  $\epsilon^{stat} = 0.5355$ .

Usually, the feed into the distillation column is the output of a superposed process unit, e.g., a chemical reactor. Changes in its operating condition directly affect the column feed. It is assumed that disturbances in the feed flow are limited to  $\pm 20\%$  of the steady-state value of 14.08l/h. Disturbances in the feed concentration are assumed to vary by a maximum of  $\pm 15\%$  of the stationary value of  $x_{methanol}^{stat} = 0.32$ . Both disturbances may very well occur as steps.

## 2.5 Operation of the plant

Industrial distillation columns are complex chemical processes. For example, there is not only the reflux-ratio and the energy-flow to influence but also the amount of

distillate taken off, the amount of bottom product taken off, the coolant flow for the condenser, the preheating of the feed and a lot more. To operate such a system is much more than just to control concentration purity. A complex process-operating-system, here a PLS80, is necessary.

The controllers considered in this paper were implemented on a MicroVAX II that is directly connected to the process-operating-system. All communication between plant, controller and operator is realized via the process-operating-system, which also supervises the 20 underlying control loops.

### 2.6 The linear model

Controller design based on the complex nonlinear model mentioned in Chapter 2.2 is hardly possible. One way to derive a controller is to use a reduced nonlinear model that exhibits the essential dynamics of the process [8] [6]. Often, these model-based design methods are only suited for a special kind of separation and require a lot of effort.

Alternatively, a controller based on a linear model can be designed. Because of the severe nonlinearities (for the same operating conditions, plant gain and dominant time constants are highly dependent on sign and size of step changes), the use of a high-order linear model yields hardly an improvement compared to a low-order model. A very simple model exhibits the essential plant dynamics well enough for control purposes.

The linear model was identified from nonlinear simulations, because we did not have access to the real distillation column until the controllers were implemented. Temperature responses on stages 14 and 28 to steps in the manipulated variable yield:

$$Y(s) = \underbrace{\begin{pmatrix} -\frac{1220}{6.1s+1} & \frac{100}{(1.2s+1)(1.5s+1)} \\ -\frac{1500}{2.7s+1} & \frac{320}{1.6s+1} \end{pmatrix}}_{G(s)} U(s) \tag{2.6.1}$$

where

$$Y(1) \dots T_{14} - T_{14}^{stat} \text{ (in Kelvin)}$$

$$Y(2) \dots T_{28} - T_{28}^{stat} \text{ (in Kelvin)}$$

$$U(1) \dots \epsilon - \epsilon^{stat}$$

$$U(2) \dots Q_E - Q_E^{stat} \text{ (in Kilowatt)}$$

Time is referenced in hours.

As gain and time constants of each transmission channel vary by up to 300% depending on the size and sign of the respective identification step input, robustness should be a main goal of linear controller design.

### 3 Controller design

Several linear controller design methods were applied to the model  $G(s)$  (eqn. 2.6.1). The resulting compensators have to meet the following design specifications:

- actuator limits (see Section 2.4)
- performance requirements (see Section 2.4)
- to achieve asymptotic rejection of disturbance steps, we require the largest singular value of the sensitivity matrix  $S$  to approach zero for small frequencies:

$$\bar{\sigma}[S] = \bar{\sigma}[(I + GK)^{-1}] \rightarrow 0 \text{ for } \omega \rightarrow 0 \quad (3.1)$$

- we require the closed loop bandwidth  $\omega_B$  (frequency, where the maximum singular value of the complementary sensitivity matrix  $T$  crosses the -3dB line) to lie between  $40 \text{ (hour)}^{-1}$  and  $50 \text{ (hour)}^{-1}$ :

$$\bar{\sigma}[T] = \bar{\sigma}[(I + GK)^{-1}GK] < -3\text{dB for } \omega > \omega_B \quad (3.2)$$

Reasons for this are:

- Suppression of measurement noise.
- Process dynamics with frequencies faster than  $\omega_B$  is completely neglected in our model; multiplicative modelling errors tend to infinity for  $\omega > \omega_B$ . Thus, in a conservative design like ours,  $\bar{\sigma}[T]$  has to drop for frequencies above  $\omega_B$  to ensure closed loop stability [1].

As usual, the process of controller design consists of four steps:

- linear design
- singular value analysis to check requirements (3.1) and (3.2)
- nonlinear simulation to check performance specifications and non-violation of actuator limits
- implementation of the controller at the real plant and - if necessary - on-line tuning.

For the first two steps we used the design packages STABLE-II [7] and KEDDC [10]. Nonlinear simulation was performed with the 42nd order model described in Section 2.3 (software package DIVA [5]).

### 3.1 $H_\infty$ -Design

The cost function to be minimized over the set of all finite-dimensional, proper and stabilizing compensator matrices  $K(s)$  is given by

$$\|H(s)\|_\infty = \max_{\omega} \bar{\sigma}[H(j\omega)] \quad (3.1.1)$$

where  $H$  is chosen as

$$H = \begin{pmatrix} W_1(s)S(s)W_2(s) \\ W_3(s)T(s)W_2(s) \\ W_4(s)K(s)S(s)W_2(s) \end{pmatrix} \quad (3.1.2)$$

and the weighting matrices  $W_2, W_4$  are:

$$W_2(s) = \text{diag}\{0, 1\} \quad (3.1.3)$$

$$W_4(s) = \text{diag}\{0.01\} \quad (3.1.4)$$

$W_1(s)$  and  $W_3(s)$  are diagonal matrices with minimum-phase entries depicted in Figure 3.1.1. This choice of weighting matrices reflects requirements (3.1) and (3.2). The entries of  $W_4$  were chosen very small, because we did not encounter any difficulties with actuator limits either in linear or nonlinear simulation. The matrices  $W_i$ ,  $i = 1, \dots, 4$  are a reasonable guess; thus, we did not need many iterations to find these particular weights. The resulting compensator is of order 8 and has three poles near  $-\infty$ . This very fast part of the compensator was approximated by nondynamic elements. Thus, we get a 5th order controller with two stable poles close to the origin, a pair of poles at  $(-0.245 \pm j0.383)$  (hour) $^{-1}$  and a pole at  $-0.617$  (hour) $^{-1}$ . Minimum and maximum singular values of  $K, S$  and  $T$  are shown in Figures 3.1.2 and 3.1.3.

Nonlinear simulation of closed loop time responses to step changes in disturbances was done. Feed flow was varied by  $\pm 20\%$ , feed concentration of component 1 by  $\pm 15\%$ . Because of lack of space, only two responses can be presented here (Figure 3.1.4 and Figure 3.1.5)). As a step change in feed flow by  $+20\%$  proved to be hardest to control, only responses of the controlled plant to this disturbance are given here (Figure 3.1.6). The controlled plant exhibited a steady-state temperature offset on the 28th tray of approximately 0.4 Kelvin. This is due to a steady decline in the feed concentration of the light-boiling component (ramp disturbance). It occurs, because in our experiments, distillate and bottom product are mixed and reused as feed. It is not anticipated that this will be a problem in industrial use. Thus, redesign was not deemed to be necessary.

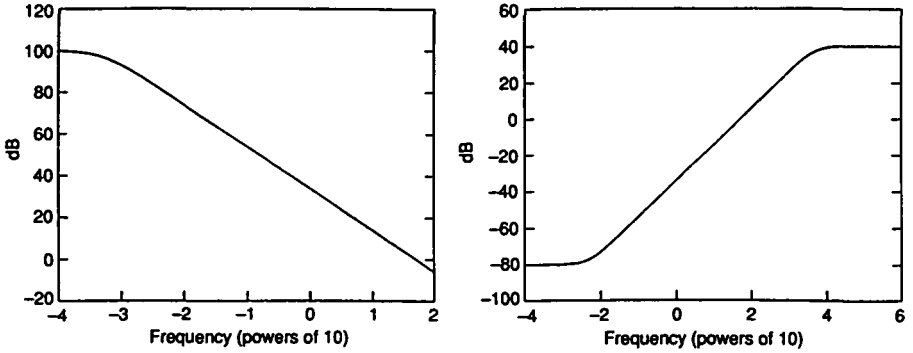


Figure 3.1.1. Elements of weighting matrices  $W_1$  and  $W_3$

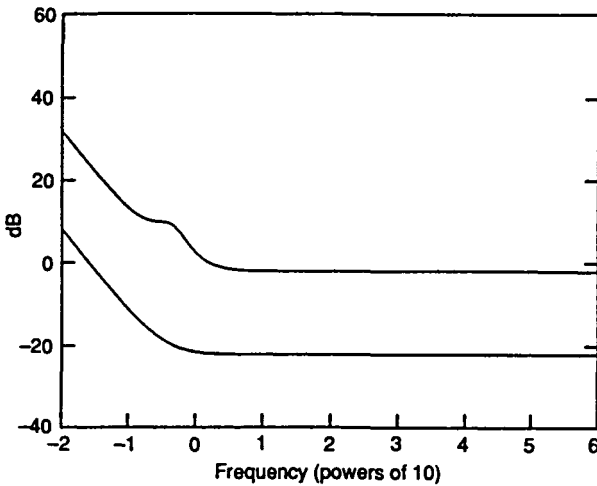


Figure 3.1.2. Minimum and maximum singular value of  $K$

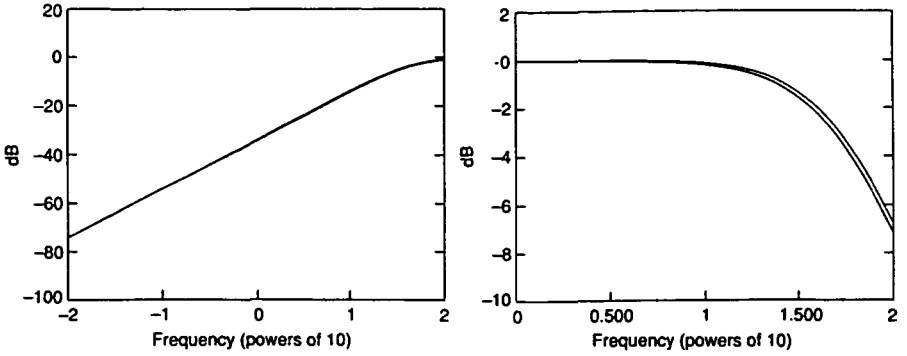


Figure 3.1.3. Minimum and maximum singular values of  $S$  and  $T$

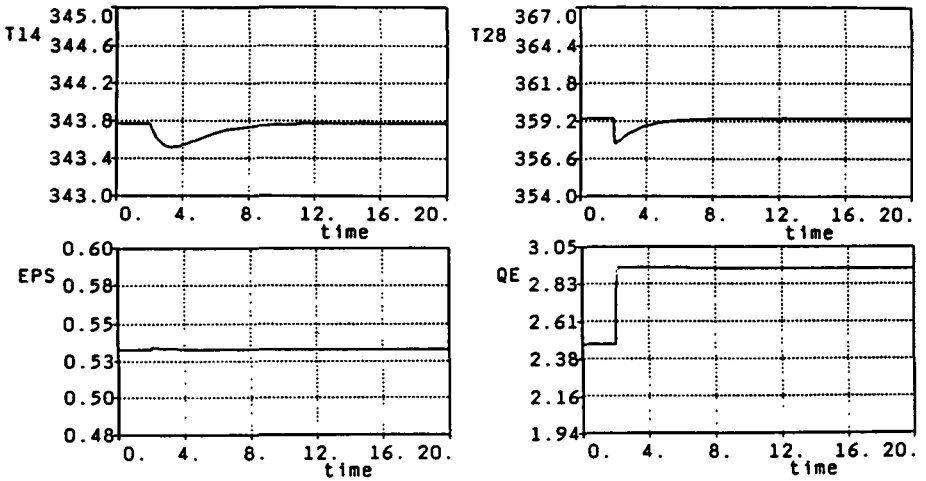


Figure 3.1.4. Responses to a step change in feed flow by +20% (simulation)

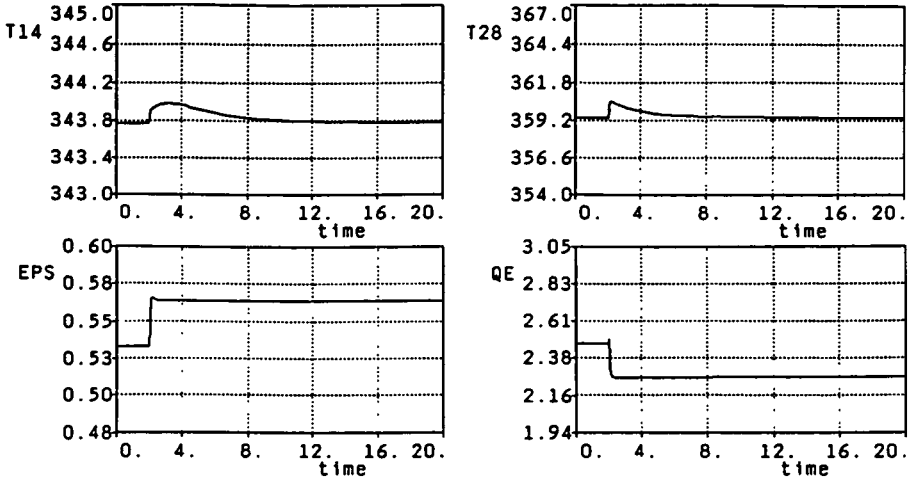


Figure 3.1.5. Responses to a step change in the feed concentration of component 1 by - 15% (simulation)

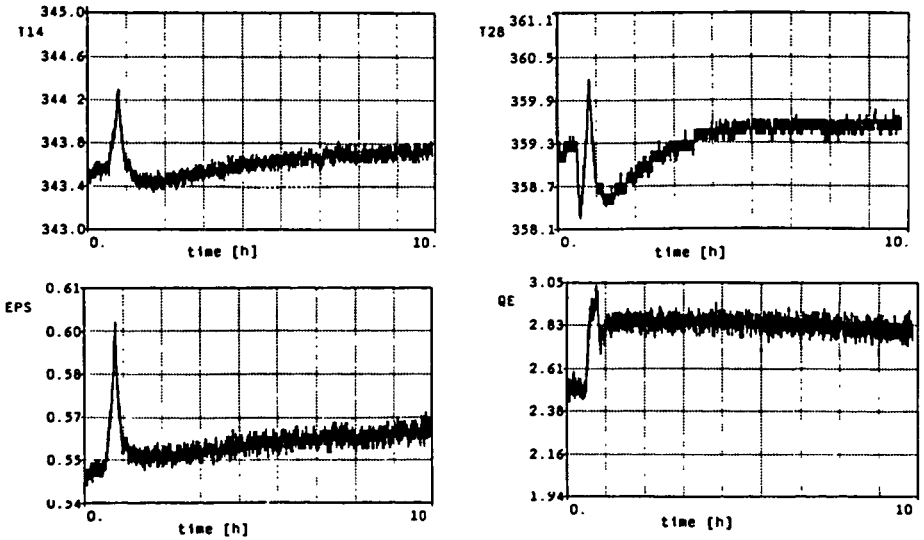


Figure 3.1.6. Responses of the controlled plant to a step change in feed flow by +20%

### 3.2 Characteristic Locus design method [4]

To achieve satisfactory closed loop performance, the characteristic locus design method relies on the manipulation of the eigenvalues (characteristic loci) and eigenvectors (characteristic directions) of the open loop frequency response matrix  $G(j\omega)K(j\omega)$ . The design proceeds in three stages:

- High-frequency alignment

At high frequencies, the characteristic directions of  $GK$  should approach the standard basis direction set. This will guarantee small high-frequency interaction between (linear) control loops. Moreover, in this frequency range, the moduli of the closed loop characteristic loci will be good approximations for the singular values of the complementary sensitivity matrix  $T$ . Good alignment is achieved by postmultiplying  $G$  with

$$K_H = \begin{pmatrix} -0.137 & 0.0 \\ -0.376 & 0.4 \end{pmatrix} \quad (3.2.1)$$

$K_H$  is obtained as a real approximation of the frame matrix of  $G^{-1}(j\omega_H)$ ,  $\omega_H = 30(\text{hour})^{-1}$ .  $K_H$  also contains appropriate scaling factors for the characteristic loci of  $G$  in this frequency range. Success of the alignment procedure can be judged from Figure 3.2.1, where the moduli of the characteristic loci and the misalignment angles between characteristic directions and standard basis vectors are shown.

- Medium-frequency adjustment

As  $\omega_B$  is well within the region of small alignment angles, closeness of open loop characteristic loci at this frequency is equivalent to closeness of  $\underline{\sigma}[T(\omega_B)]$  and  $\bar{\sigma}[T(\omega_B)]$ . This is achieved fairly (but not very) well through an additional compensator

$$K_M(s) = A \begin{pmatrix} k_M(s) & 0.0 \\ 0.0 & 1.0 \end{pmatrix} A^{-1} \quad (3.2.2)$$

where  $A$  is a real approximation to the eigenvector frame of  $G(j\omega_M)K_H$ ,  $\omega_M = 20(\text{hour})^{-1}$  and  $k_M$  is a first-order lag with corner frequency  $10(\text{hour})^{-1}$  and attenuation 9.5dB. The result of this loci adjustment procedure can be checked from the Nyquist plots in Figure 3.2.2.

- Low-frequency compensation

At this stage, we inject additional low-frequency gain into the loops and balance up the moduli of the characteristic loci in the low-frequency range. This is accomplished by an additional compensator

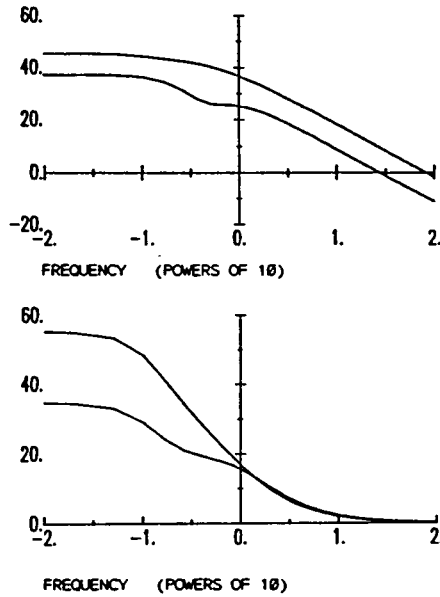


Figure 3.2.1. Moduli of characteristic loci and misalignment angles after high-frequency compensation

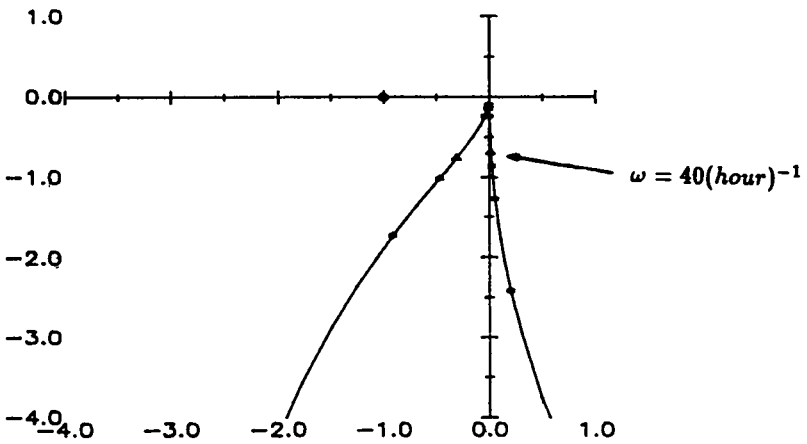


Figure 3.2.2. Characteristic loci after medium-frequency adjustment

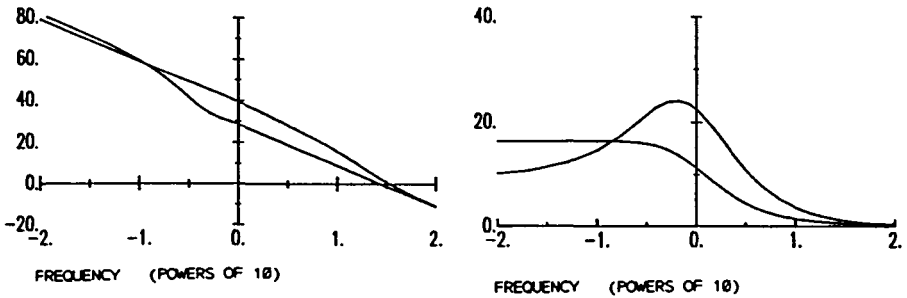


Figure 3.2.3. Moduli of characteristic loci and misalignment angles of  $GK$

$$K_L(s) = \frac{1}{s} B \begin{pmatrix} 1.5 & 0.0 \\ 0.0 & 0.5 \end{pmatrix} B^{-1} + I \tag{3.2.3}$$

where  $B$  is a real approximation to the eigenvector frame of  $GK_H K_M$  at  $\omega_L = 0.1$  (hour)<sup>-1</sup>.

Thus, the result of this design is a third order controller with two poles at the origin and one pole at  $s = -10$  (hour)<sup>-1</sup>. Moduli of the open loop characteristic loci and misalignment plots are shown in Figure 3.2.3. Minimum and maximum singular values of  $S$  and  $T$  are given in Figure 3.2.4.

Nonlinear simulation of closed loop time responses and real responses of the controlled plant to a step change in feed flow are presented in Figures 3.2.5. and 3.2.6. Due to a software error, data acquisition was stopped too early. The controlled plant exhibited a steady-state temperature offset on the 28th tray of approximately 0.5 K. For the same reasons as in Section 3.1, this is not considered to be a problem. Thus, additional integral action was not included in the controller. Steady states of the manipulated variables are different from those in Figure 3.1.6. This is also due to the decline in the feed concentration of the light-boiling component.

### 3.3 Direct Nyquist array design method [9]

In DNA design, the multivariable problem is reduced to a number of scalar problems by introducing a suitable 'nearly decoupling' precompensator  $K_P$ . Especially,

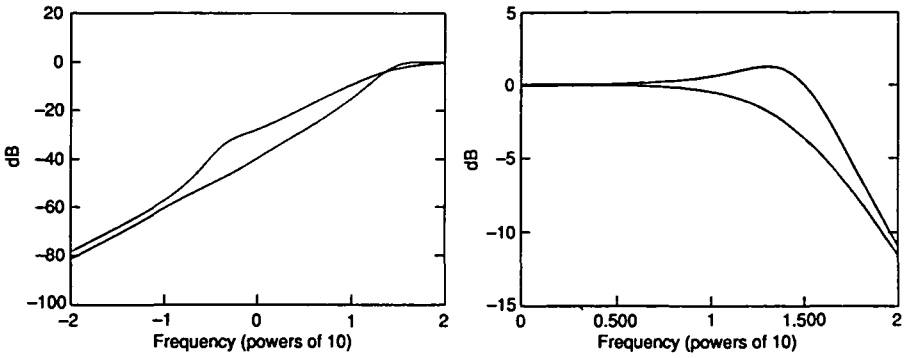


Figure 3.2.4. Minimum and maximum singular values of  $S$  and  $T$

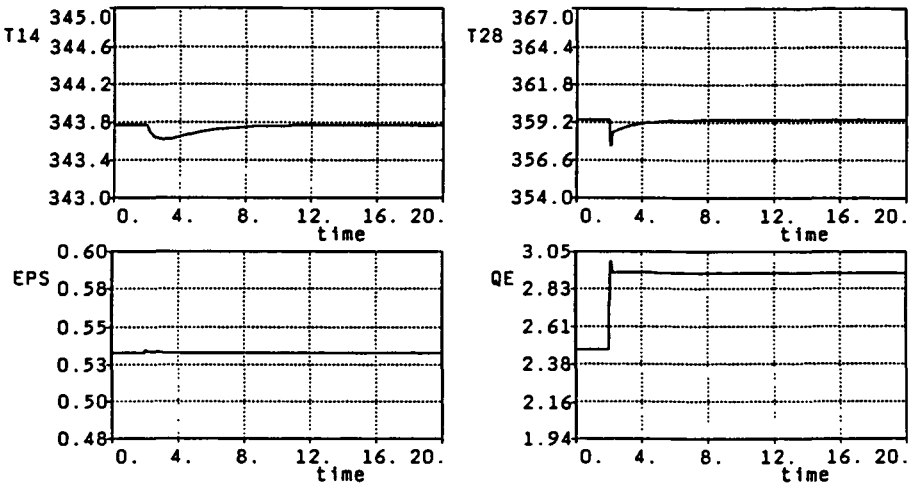


Figure 3.2.5. Responses to a step change in feed flow by +20% (simulation)

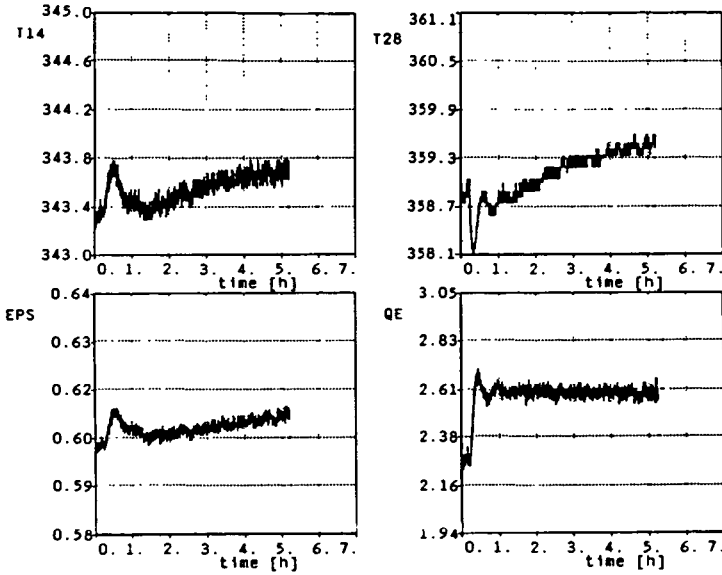


Figure 3.2.6. Responses of the controlled plant to a step change in feed flow by +20%

if  $G(j\omega)K_P(j\omega)$  is column diagonal dominant, two scalar controllers  $k_{C_1}(s)$  and  $k_{C_2}$  stabilizing their individual loops will guarantee that

$$K_C(s) = \begin{pmatrix} k_{C_1}(s) & 0.0 \\ 0.0 & k_{C_2} \end{pmatrix} \tag{3.3.1}$$

stabilizes the multivariable control system.

The precompensator matrix  $K_P(s)$  was chosen as

$$K_P(s) = \begin{pmatrix} -\frac{0.135 + 0.365s}{0.625 + s} & 1 \\ -1 & 12.17 \end{pmatrix} \tag{3.3.2}$$

From Figure 3.3.1 it is clear that the uncompensated system is not column diagonal dominant, whereas for the compensated system diagonal dominance is achieved (Figure 3.3.2). Thus, scalar controller design for the two diagonal elements of  $G(s)K_P(s)$  is justified. For both systems, we choose PI controllers

$$K_{C_1}(s) = 0.562 \frac{1+s}{s} \tag{3.3.3}$$

$$K_{C_2}(s) = 0.013 \frac{1+s}{s} \tag{3.3.4}$$

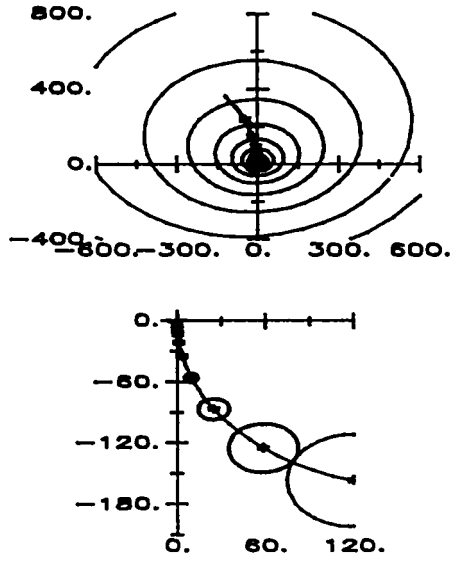


Figure 3.3.1. Gershgorin bands of uncompensated system

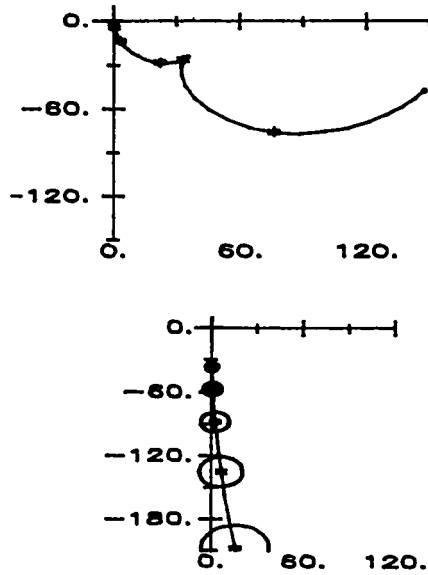


Figure 3.3.2. Gershgorin bands of compensated system

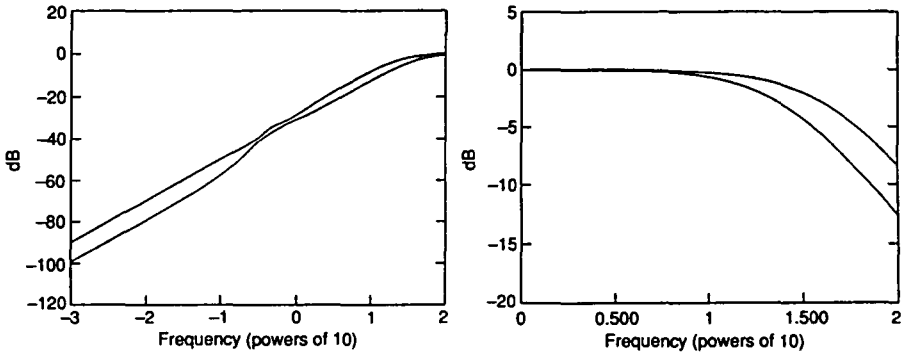


Figure 3.3.3. Minimum and maximum singular values of  $S$  and  $T$

Apart from introducing integral action, they approximately balance up open loop gains.

Minimum and maximum singular values of  $S$  and  $T$  are given in Figure 3.3.3.

Nonlinear simulation of closed loop time responses and real responses of the controlled plant to a step change in feed flow are presented in Figures 3.3.4 and 3.3.5.

### 3.4 $H_2$ -Minimization [11]

The cost function to be minimized is given by

$$\|H\|_2 = \sqrt{\frac{1}{2\pi} \int_{-\infty}^{+\infty} \text{tr}[H^*(j\omega)H(j\omega)] d\omega} \quad (3.4.1)$$

and  $H$  is the same as in Chapter 3.1. The resulting compensator is of order 8 and has two poles near  $-\infty$ . Those very fast modes were approximated by nondynamic elements. Thus, we end up with a 6th order controller with two poles close to the origin, a pair of poles at  $(-0.245 \pm j0.383)(\text{hour})^{-1}$  and two poles at  $-55.2(\text{hour})^{-1}$ .

Maximum and minimum singular values of the  $H_2$ -controller matrix in Figure 3.4.1 should be compared to those of the  $H_\infty$ -controller. Maximum and minimum singular values of  $S$  and  $T$  are given in Figure 3.4.2.

Unfortunately, we did not have the opportunity to implement this controller at the plant. Thus, only simulation results are given (Figure 3.4.3).

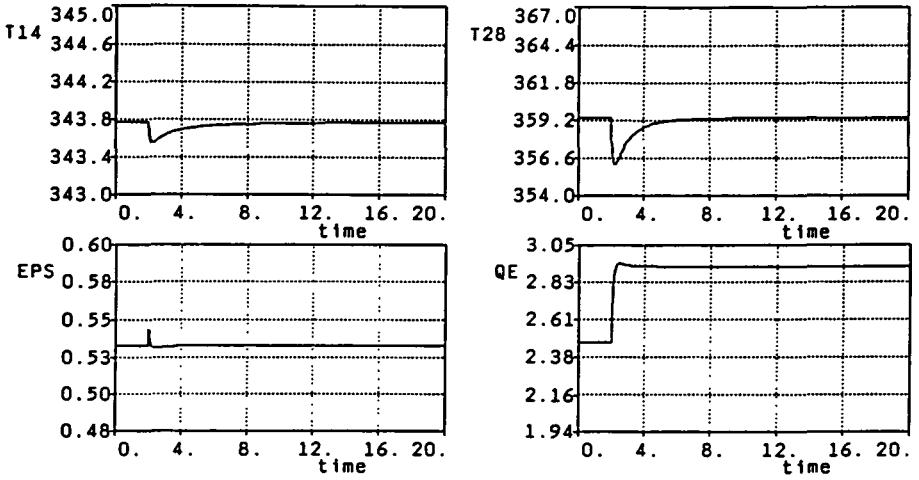


Figure 3.3.4. Responses to a step change in feed flow by +20% (simulation)

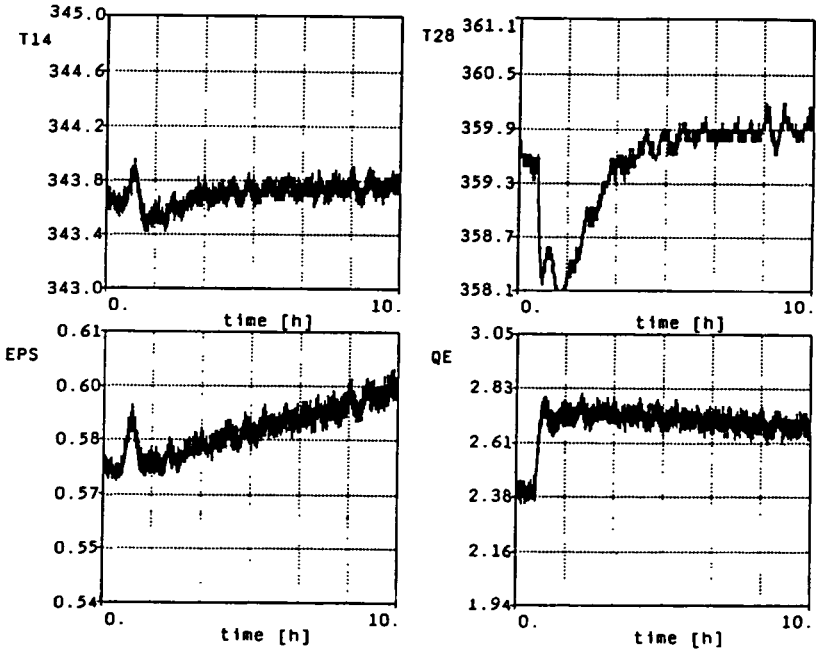


Figure 3.3.5. Responses of the controlled plant to a step change in feed flow by +20%

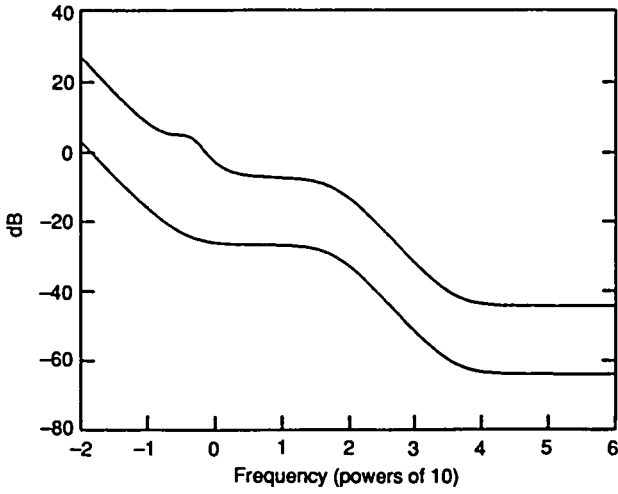


Figure 3.4.1. Minimum and maximum singular value of  $K$

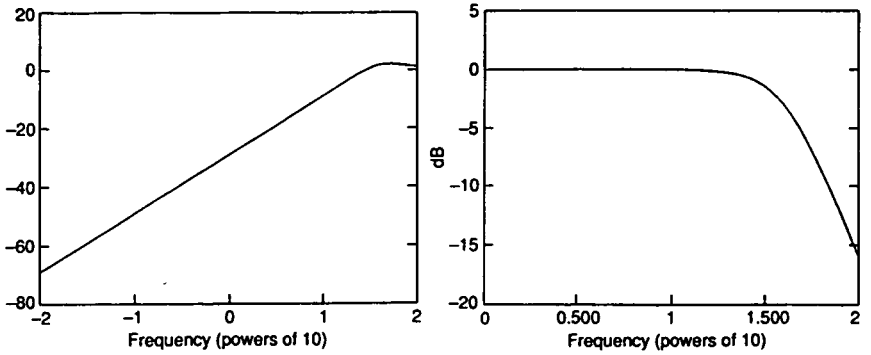


Figure 3.4.2. Minimum and maximum singular values of  $S$  and  $T$

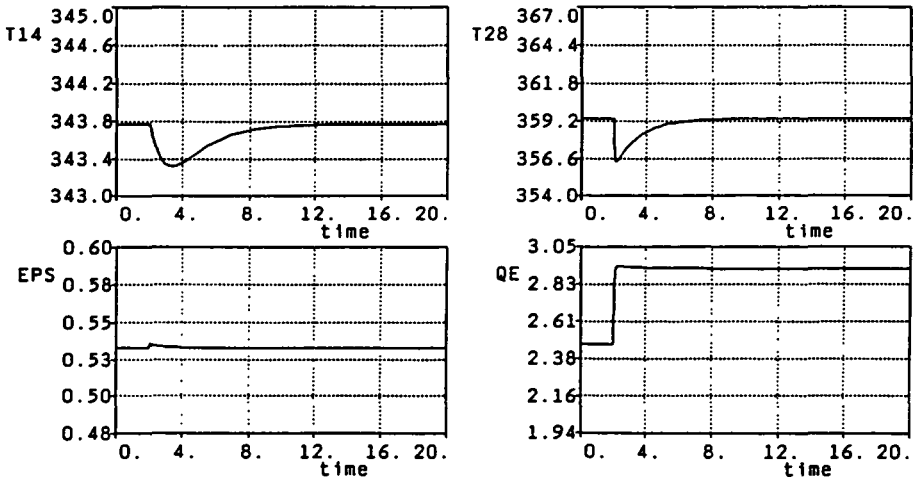


Figure 3.4.3. Responses to a step change in feed flow by +20% (simulation)

### 3.5 Conventional PI-design

For comparison with the multivariable techniques of the preceding chapters, we have designed conventional PI-controllers  $k_1$  and  $k_2$  for the diagonal elements  $g_1(s)$  and  $g_2(s)$  of  $G(s)$ . They were chosen to approximately balance up the gains of  $g_1$  and  $g_2$ . The gains of  $g_1 k_1$  and  $g_2 k_2$  are shown in Figure 3.5.1. Maximum and minimum singular values of  $S$  and  $T$  are given in Figure 3.5.2. Nonlinear simulation of time responses to a step change in feed flow is presented in Figure 3.5.3. The drop in temperature  $T_{28}$  is only stopped, when the profile moves into the bottom. This is reflected in a remarkable decrease of bottom purity (Figure 3.5.4). Qualitatively the same behaviour was observed, when the PI-controllers were implemented at the distillation plant. There, however, an even smaller decrease in  $T_{28}$  resulted in impurity of the bottom product.

## 4 Conclusions

All controllers obtained by multivariable design methods work well in nonlinear simulation and achieve satisfactory performance at the real plant. This is, however, not true for the conventional PI-controllers.

As our designs are conservative, there is considerable scope for on-line tuning of controller parameters. This has been done. As expected, it improves performance. It has to be stressed, however, that - with the exception of the decoupled PI-

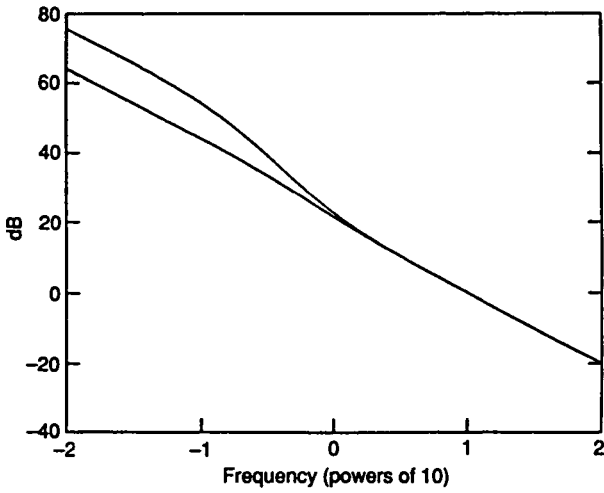


Figure 3.5.1. Gain of  $g_1k_1$  and  $g_2k_2$

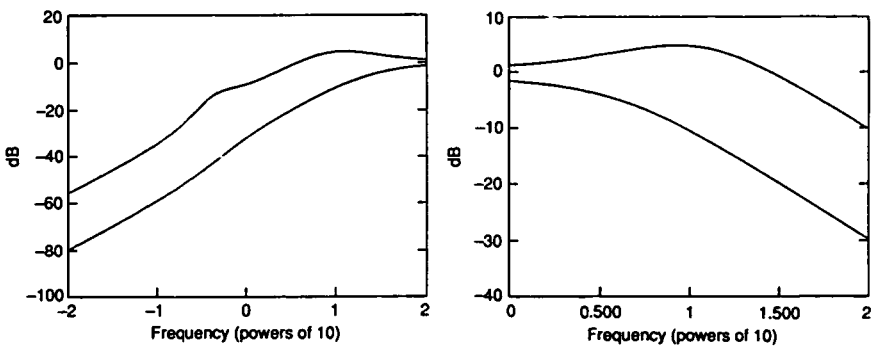


Figure 3.5.2. Minimum and maximum singular values of  $S$  and  $T$

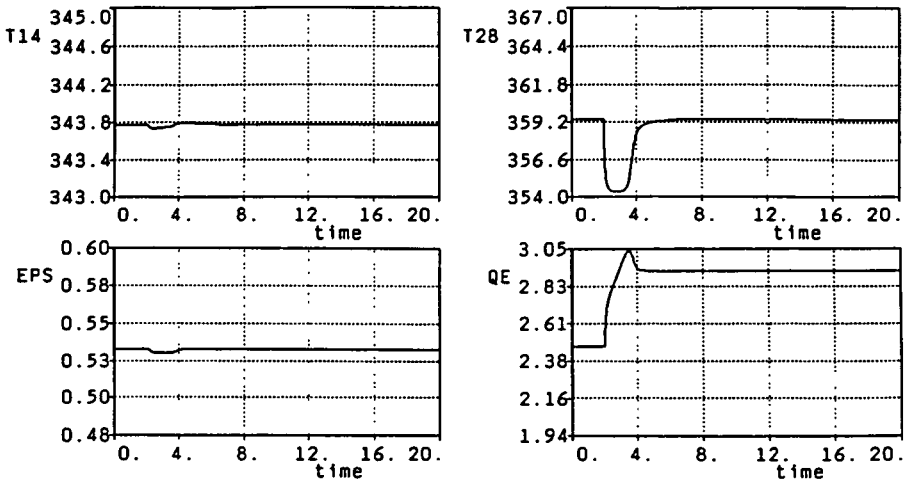


Figure 3.5.3. Responses to a step change in feed flow by +20% (simulation)

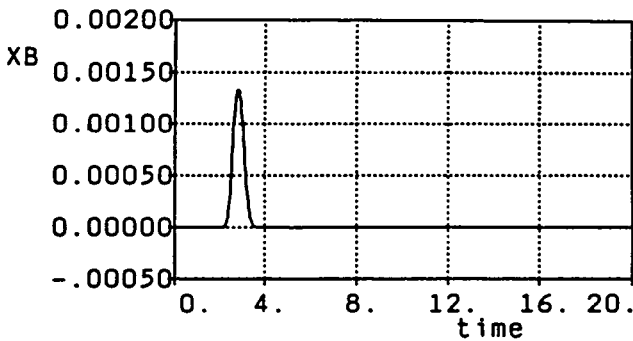


Figure 3.5.4. Bottom concentration of component 1 (simulation)

controllers - on-line tuning is not necessary to meet performance specifications. Thus, the results are not given here.

For the disturbances considered in this paper, it is possible to trade off increased design effort (multivariable design) and on-line tuning (conventional PI-design). If, however, a situation occurs, where both multivariable design and on-line tuning are necessary, one would probably favour DNA or CL controllers; they can be tuned more easily than  $H_2$  or  $H_\infty$  controllers.

If there is no need for on-line tuning, it is difficult to tell which multivariable design method is easiest to handle. It seems to be pretty much a question of personal preference and experience. In our case (comparably low level of experience with any multivariable design), the amount of time necessary to achieve satisfactory results was about the same for each method.

## Acknowledgements

Thanks are due to L. Lang, M. Wurst, A. Kröner, P. Holl, H. P. Kurrle and E. Hensel.

## References

- [1] John C. Doyle and Gunter Stein. Multivariable feedback design: concepts for a classical/modern synthesis. *IEEE Transactions on Automatic Control*, 26:4-16, 1981.
- [2] Bruce A. Francis. *A Course in  $H_\infty$  Control Theory*. Springer-Verlag, Berlin, 1987.
- [3] Bruce A. Francis and John C. Doyle. Linear control theory with an  $H_\infty$  optimality criterion. *SIAM Journal on Control and Optimization*, 25:815-844, 1987.
- [4] A. G. J. MacFarlane and B. Kouvaritakis. A design technique for linear multivariable feedback systems. *International Journal of Control*, 25:837-874, 1977.
- [5] W. Marquardt, P. Holl, D. Butz, and E. D. Gilles. DIVA, a flow-sheet oriented dynamic process simulator. *Chemical Engineering & Technology*, 10:164-173, 1987.
- [6] Wolfgang Marquardt. *Nichtlineare wellenausbreitung - Ein Weg zu reduzierten dynamischen Modellen von Stofftrennprozessen*. VDI Verlag, Düsseldorf, 1988.
- [7] Ian Postlethwaite, S. D. O'Young, and D.-W. Gu, *stabe-H User's Guide*. Technical Report, University of Oxford, 1987.
- [8] B. Retzbach. *Mathematische Modelle von Destillationskolonnen zur Synthese von Regelungskonzepten*. VDI Verlag, Düsseldorf, 1986.

- [9] H. H. Rosenbrock, *Computer-Aided Control Systems Design*. Academic Press, London, 1974.
- [10] C. Schmid, *KEDDC Benutzerhandbuch*. Technical Report, Ruhr-Universität Bochum, 1987.
- [11] G. Stein and M. Athans. The LQG/LTR procedure for multivariable feedback control design. *IEEE Transactions on Automatic Control*, 32:105-114, 1987.